Research Article

Journal of Environmental Nanotechnology

Visible-light Driven Photocatalytic Degradation of Rhodamine B over Ce-g-C_3N_4 Composite: Structure - Activity Relationship Study

C. Kalaiyarasi[1], P. Dhilip[2], A. Dhivya[3], P. Mahalingam[4], Smagul Karazhanov[4] and P. Sivakumar[5*]

[1]Department of Chemistry, Arignar Anna Government Arts College, Namakkal, TN, India.
[2] Department of Chemistry, Bannari Amman Institute of Technology, Sathyamangalam, Erode, TN, India
[3] Department of Chemistry, Muthayammal College of Arts and Science, Rasipuram, TN, India
[4]Leading Researcher, Thin Film Laboratory, Institute of Solid State Physics, UL Kengarag, Riga
[5] Department of Chemistry, Government Arts and Science College, Komarapalayam, TN, India
Received: 07.06.2026 Accepted: 15.07.2026 Published: xx.xx.xxxx
*shivagobi@gmail.com

ABSTRACT

Graphitic carbon nitride (g-C_3N_4) has emerged as a promising visible-light-responsive photocatalyst for wastewater treatment. However, its practical application is hindered by limited visible-light absorption and the rapid recombination of photogenerated charge carriers. In the present study, a cerium-modified graphitic carbon nitride composite (Ce-g-C_3N_4) was synthesized through a hydrothermal route to improve the photocatalytic degradation of Rhodamine B (RhB) under visible-light irradiation. The structural, morphological, and optical properties of the prepared materials were investigated using XRD, FTIR, UV-Vis spectroscopy, and SEM-EDS analyses. UV-Vis analysis revealed a reduced band gap energy of 2.59 eV for Ce-g-C_3N_4, indicating enhanced visible-light absorption compared with pristine g-C_3N_4. SEM observations showed a fragmented sheet-like morphology with a rough surface texture, which is favourable for dye adsorption and photocatalytic reactions. The effects of catalyst dosage, initial dye concentration, solution pH, and irradiation time on RhB degradation were systematically evaluated. Under the optimized conditions of 30 mg catalyst dosage, 50 ppm RhB concentration, and pH 9.5, the Ce-g-C_3N_4 composite achieved a maximum degradation efficiency of 89.1% within 70 min, whereas pristine g-C_3N_4 exhibited only 69.7% degradation under identical conditions. The degradation process followed pseudo-first-order kinetics with an apparent rate constant of 0.0324 min^{-1} and a correlation coefficient (R^2) of 0.9897. In addition, the photocatalyst retained 81.2% of its initial activity after five consecutive cycles, demonstrating good stability and reusability. The improved photocatalytic performance is attributed to the modification of the electronic structure and enhanced visible-light utilization induced by cerium incorporation. These findings demonstrate that Ce-g-C_3N_4 is an efficient and stable visible-light-responsive photocatalyst with potential applications for treating dye-contaminated wastewater.

Keywords: Rhodamine B; Ce-g-C_3N_4 composite; Photocatalysis; Visible-light photocatalyst; Wastewater treatment; Rare-earth doping.

1. INTRODUCTION

Graphitic carbon nitride (g-C_3N_4) has emerged as one of the most promising light-responsive photocatalysts because of its suitable band gap, excellent physicochemical stability, low toxicity, and simple preparation route. Nevertheless, the practical application of pristine g-C_3N_4 remains restricted by its limited visible-light absorption, low specific surface area, and rapid recombination of photogenerated electron-hole pairs, which significantly reduce its photocatalytic efficiency. To address these limitations, several approaches to modification, including elemental doping, heterojunction formation, defect engineering, and morphology control, have been explored. Among these methods, elemental doping is considered particularly effective because it can tune the electronic structure of g-C_3N_4, create additional active sites, and enhance charge-separation efficiency (Pan *et al.* 2020; Pratikshya *et al.* 2026). Cerium has attracted considerable attention as a dopant due to its unique Ce^{3+}/Ce^{4+} redox couple and partially filled 4f orbitals, which can act as electron-trapping centres and facilitate interfacial charge transfer. Previous studies have demonstrated that incorporating Ce species into g-C_3N_4 can improve visible-light absorption and photocatalytic activity (Guo *et al.* 2021; Khansaa *et al.* 2025; Kesarla *et al.* 2019). However, several challenges still remain. In many reported Ce/g-C_3N_4 systems, the interaction between cerium species and the g-C_3N_4 framework remains insufficiently elucidated, and the relationship between structural modification and photocatalytic performance is still not fully understood. Furthermore, most studies have focused primarily on the degradation of pollutants at relatively low dye concentrations, which do not adequately represent the pollutant levels commonly

encountered in industrial wastewater. Therefore, the development of a stable and efficient Ce-g-C_3N_4 photocatalyst capable of operating under relatively concentrated dye conditions remains an important research challenge. Rhodamine B (RhB) was selected as the target pollutant in this study because it is one of the most widely used xanthene dyes in textile, paper, and printing industries and is frequently detected in industrial wastewater. RhB possesses a complex aromatic structure and high chemical stability, making it resistant to conventional treatment methods and suitable as a model compound for evaluating photocatalytic performance (Rafiq *et al.* 2021; Khan *et al.* 2025). Moreover, the degradation of RhB has been widely used as a benchmark reaction to compare the efficiency of newly developed photocatalysts because changes in its concentration can be easily monitored by UV-visible spectroscopy. The concentration range of 30–70 ppm was selected to simulate moderately concentrated dye-containing wastewater and to evaluate the catalytic performance of Ce-g-C_3N_4 under more realistic conditions than those commonly reported in previous studies (Pattanayak *et al.* 2024; Manoj *et al.* 2025).

In the present work, Ce-g-C_3N_4 was synthesized through a simple calcination-assisted hydrothermal method and systematically investigated for the visible-light-driven degradation of Rhodamine B. The structural, morphological, and optical properties of the prepared materials were correlated with their photocatalytic performance to elucidate the role of cerium incorporation in improving charge separation and visible-light utilization. The novelty of this work lies in the development of an efficient Ce-g-C_3N_4 photocatalyst that exhibits enhanced photocatalytic activity and good stability at relatively high RhB concentrations, along with a detailed study of the structure-activity relationship. The findings of this study provide further insight into the design of rare-earth-modified g-C_3N_4 photocatalysts and offer a promising strategy for treating dye-contaminated wastewater under visible-light irradiation (Anjana *et al.* 2025; Alsalmah *et al.* 2025).

2. MATERIALS AND METHODOLOGY

2.1 Required Chemicals

All chemicals in this work were commercially available and used without any further purification. Melamine (99%), cerium (III) nitrate hexahydrate ($Ce(NO_3)_3 \cdot 6H_2O$, 99.5%), ethanol (C_2H_5OH), nitric acid (HNO_3), and ammonia solution (NH_4OH) were procured from Aldrich Chemical Company Limited, UK, and are of analytical grade.

2.2 Synthesis of g-C_3N_4

Graphitic carbon nitride (g-C_3N_4) was synthesized by the thermal polymerization of melamine. Briefly, 5 g of melamine was placed in a covered alumina crucible and heated in a muffle furnace from room temperature to 550 °C at a heating rate of 5 °C min^{-1}. The sample was maintained at 550 °C for 2 h to ensure complete condensation of the melamine precursor into the polymeric g-C_3N_4 framework. After calcination, the furnace was allowed to cool naturally to room temperature. The obtained yellow product was collected and ground into a fine powder using an agate mortar and pestle for further use.

2.3 Synthesis of CeO_2 Particles

Cerium oxide (CeO_2) was synthesized by a precipitation method. An aqueous 0.2 M solution of $Ce(NO_3)_3 \cdot 6H_2O$ was prepared and continuously stirred in a 1 L beaker at 80 °C for 60 min. The pH of the solution was then adjusted to 10 by dropwise addition of NH_4OH, followed by 120 min of stirring to ensure complete precipitation. After completion of the reaction, the mixture was cooled to 30°C, and the resulting precipitate was collected by filtration. The precipitate was washed repeatedly with deionized water and ethanol until a neutral pH was attained. The filtered product was dried in an oven at 105°C for 5 h and subsequently calcined at 550°C for 3 h in a furnace. The obtained CeO_2 powder was finally cooled in a desiccator and stored for further use.

2.4 Synthesis of Ce-g-C_3N_4 Composite

Ce-g-C_3N_4 composite was synthesized by a hydrothermal method. Initially, 2 g of CeO_2 and 2 g of g-C_3N_4 were separately dispersed in 100 mL of deionized water by ultrasonication for 60 min. The CeO2-to-g-C_3N_4 weight ratio was fixed at 1:1 (50 wt.% CeO2) to ensure sufficient interfacial contact between the components and to promote efficient charge transfer across the heterojunction. Previous studies have shown that the photocatalytic performance of CeO_2/g-C_3N_4 composites strongly depends on the degree of interfacial coupling and the relative composition of both phases (Guo *et al.* 2021; Devi *et al.* 2026). Therefore, an equal weight ratio was selected to maximize heterojunction interactions and investigate the structure-activity relationship of the composite.

The two suspensions were mixed and sonicated for an additional 60 min to obtain a homogeneous dispersion. The resulting suspension was transferred into a 250 mL Teflon-lined stainless-steel autoclave and maintained at 180 °C for 4 h. During the hydrothermal process, CeO_2 nanoparticles were uniformly anchored to the layered g-C_3N_4 surface via electrostatic interactions and interfacial bonding, resulting in intimate contact between the two semiconductors. Such interfacial interaction facilitates the migration of photogenerated charge carriers and suppresses electron-hole recombination, thereby improving photocatalytic

performance. After completion of the reaction, the autoclave was allowed to cool naturally to room temperature. The product was recovered by centrifugation at 5000 rpm for 10 min, washed three times with deionized water and ethanol to remove residual impurities, and dried at 105 °C for 3 h. Finally, the obtained material was annealed at 400 °C for 2 h and stored in an airtight container for further characterization and photocatalytic studies.

2.5 Photocatalytic Process

Photocatalytic degradation experiments were carried out in a cylindrical glass batch reactor containing 100 mL of Rhodamine B (RhB) solution. RhB solutions with initial concentrations of 30, 40, 50, 60, and 70 ppm were prepared by dissolving the appropriate amount of dye in distilled water. The selected concentration range was intended to simulate moderately concentrated dye-containing wastewater and to evaluate catalytic performance under conditions closer to those of real industrial effluents. A measured amount of Ce-g-C_3N_4 photocatalyst (10, 20, 30, 40, and 50 mg) was dispersed in the dye solution by ultrasonication. Before irradiation, the suspension was magnetically stirred in the dark for 30 min to establish adsorption-desorption equilibrium between the dye molecules and the catalyst surface.

Visible-light irradiation was provided by a phosphor-coated mercury vapour lamp (300 W) with an emission wavelength range of 400–550 nm. The lamp was positioned vertically at a fixed distance of 25 cm above the reactor. Throughout the experiment, the reaction mixture was continuously stirred, and the temperature was maintained at 25 ± 2 °C by natural air cooling. During the photocatalytic reaction, 15 mL aliquots were withdrawn at regular intervals and immediately centrifuged at 5000 rpm for 10 min to remove suspended catalyst particles. The residual RhB concentration was determined using a UV-visible spectrophotometer by monitoring the characteristic absorption peak of RhB at 554 nm. The degradation efficiency was calculated using Eq. (1).

$$\text{Degradation efficiency (\%)} = A_0\text{-}A_t/A_0 \times 100 \ldots (1)$$

where A_0 represents the initial concentration of Rhodamine B, and A_t denotes the concentration of Rhodamine B at irradiation time *t*. This expression was used to determine the percentage degradation of the dye during the photocatalytic process. The adopted procedure enabled an accurate evaluation of the photocatalytic performance of the prepared material under controlled experimental conditions. In addition, the obtained results provided useful information related to the degradation kinetics and the possible reaction mechanism of Rhodamine B under visible-light irradiation.

For the recyclability experiments, the used catalyst was recovered by centrifugation at 5000 rpm for 10 min, washed thoroughly with deionized water and ethanol to remove adsorbed intermediates, and dried at 80 °C for 6 h before reuse in the subsequent cycle. The recovered catalyst was then employed under identical experimental conditions to evaluate its stability and reusability.

3. RESULTS AND DISCUSSION

3.1 XRD Analysis

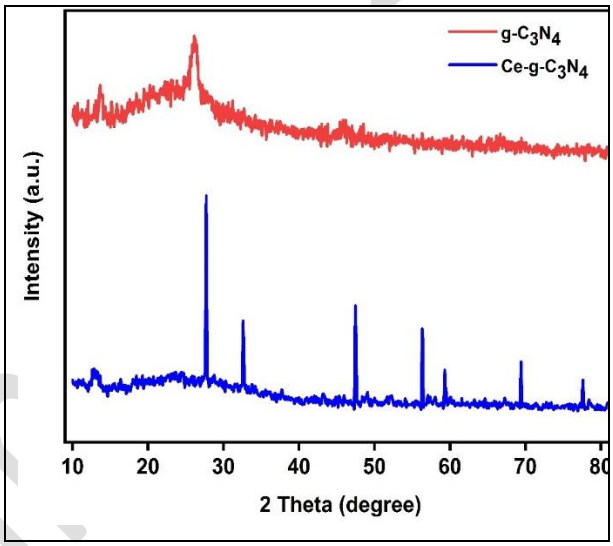

Fig. 1: Shows the XRD patterns of g-C_3N_4 and Ce-g-C_3N_4 composite

The XRD patterns of the synthesized g-C_3N_4 and Ce-g-C_3N_4 samples are presented in Fig. 1. Pristine g-C_3N_4 exhibits two characteristic diffraction peaks at 2θ values of 13.78° and 27.26°, corresponding to the (100) and (002) crystal planes, respectively. The peak at 13.78° is associated with the in-plane structural packing of tri-s-triazine units, whereas the peak at 27.26° arises from interlayer stacking of the conjugated aromatic framework. These reflections are in good agreement with JCPDS No. 87-1526, confirming the successful formation of hexagonal g-C_3N_4. The average crystallite size calculated from the Debye-Scherrer equation was approximately 41.5 nm (Adewuyi and Oderinde, 2024).

For the Ce-g-C_3N_4 composite, additional diffraction peaks were observed at 2θ values of 27.84°, 32.67°, 47.30°, and 56.30°, which correspond to the (111), (200), (220), and (311) planes of cubic CeO_2, respectively, consistent with JCPDS card No. 81-0792. The appearance of these peaks confirms the successful incorporation of crystalline CeO_2 into the g-C_3N_4 matrix. The reduced intensity or partial disappearance of the characteristic g-C_3N_4 peaks after composite formation may be attributed to structural distortion of sp^2-bonded carbon sites and partial loss of long-range ordering during the synthesis process. These results suggest strong

interfacial contact between CeO_2 and g-C_3N_4, with CeO_2 particles distributed not only on the surface but also within the layered structure of g-C_3N_4.

The crystallite size of the Ce- g-C_3N_4 composite was estimated using the Debye-Scherrer equation based on the X-ray wavelength (λ = 0.154nm), the full width at half maximum (β), K is the shape factor (0.9), and the Bragg angle (θ) (Kalaiyarasi *et al.* 2026).

$$D = K\lambda/\beta\cos\theta \quad \ldots (2)$$

The average crystallite size was calculated to be 35.12 nm, which is smaller than that of pristine g-C_3N_4. The reduction in crystallite size may increase the number of exposed active sites and shorten diffusion pathways for charge carriers, thereby improving photocatalytic activity. The crystallite sizes calculated using the Debye-Scherrer equation should be regarded as approximate because the broadening of XRD peaks can also be influenced by lattice strain, crystal defects, and structural disorder (Ahmed *et al.* 2012).

3.2 FTIR Analy

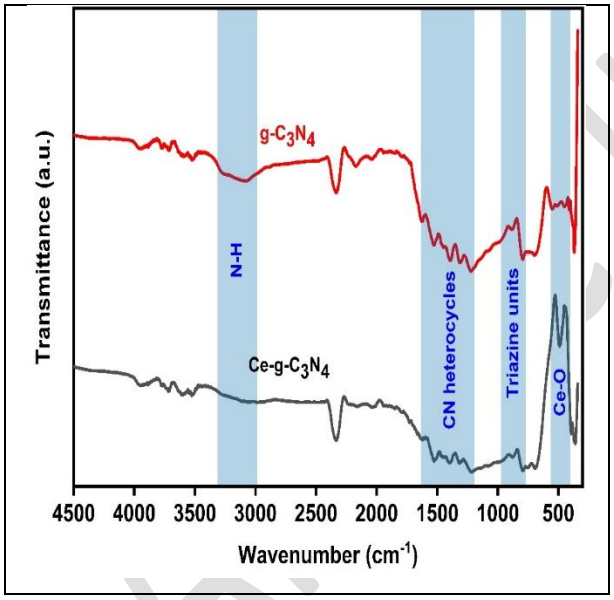

Fig. 2: Shows the FTIR spectra of g-C3N4 and Ce- g-C3N4 composite

The FTIR spectra of g-C_3N_4 and Ce-g-C_3N_4 composite were recorded in the range of 500–4500 cm^{-1} to identify the functional groups present on the surface of the prepared samples. As shown in Fig. 2, pristine g-C_3N_4 exhibits the characteristic absorption bands of graphitic carbon nitride, confirming its successful formation. A broad band observed in the region of 3000–3300 cm^{-1} is attributed to N–H stretching vibrations arising from residual amino groups or incomplete condensation of precursor species.

The series of absorption peaks between 1200 and 1620 cm^{-1} corresponds to the stretching vibrations of aromatic C–N and C=N bonds within the heterocyclic framework of g-C_3N_4. In addition, the distinct peak near 845 cm^{-1} is assigned to the breathing mode of the tri-s-triazine ring, which is a typical structural feature of graphitic carbon nitride. For the Ce-g-C_3N_4 composite, a broad absorption band centered at 3078 cm^{-1} is associated with the stretching vibration of residual N–H groups. The peaks observed in the range of 1200–1600 cm^{-1}, particularly at 1280, 1362, and 1588 cm^{-1}, are attributed to C–NH–C, C–N, and C=N stretching vibrations, respectively, confirming that the g-C_3N_4 framework was retained after Ce incorporation. A slight shift of the characteristic g-C_3N_4 bands toward lower wavenumbers, together with reduced peak intensity, indicates electronic interaction between cerium species and the g-C_3N_4 matrix, which may weaken the C–N and C=N bonds. Furthermore, the absorption bands at 522 and 450 cm^{-1} are assigned to Ce–O vibrations, confirming the presence of cerium oxide species in the composite. The preservation of the main g-C_3N_4 bands in the composite demonstrates that the fundamental structure of graphitic carbon nitride remained intact after modification (Alosaimi *et al.* 2021).

3.3 UV – Vis Analysis

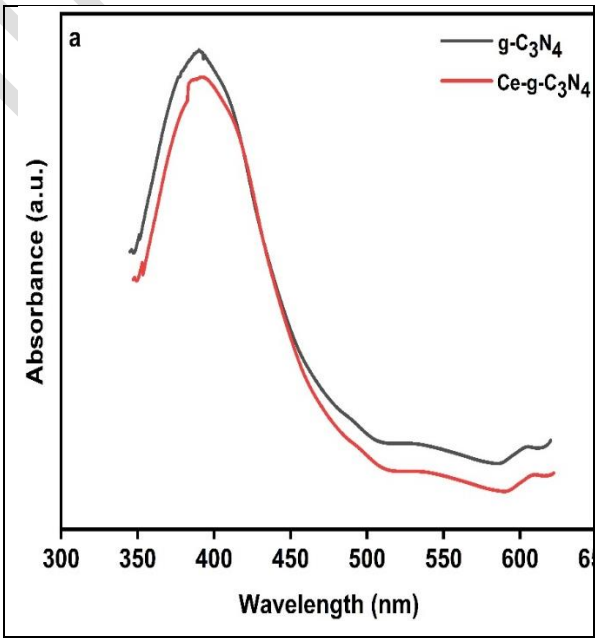

Fig. 3a: Shows the UV–Vis absorption spectra of g-C3N4 and Ce- g-C3N4 composite

The UV-visible absorption spectra of pristine g-C_3N_4 and Ce-g-C_3N_4 composite are presented in Fig. 3a. Pristine g-C_3N_4 exhibits its characteristic absorption in the UV-visible region, with an absorption edge located near 400 nm, which is consistent with the intrinsic electronic transition of graphitic carbon nitride (Wudil *et al.* 2023). After cerium incorporation, the Ce-g-C_3N_4

composite exhibits a pronounced redshift in the absorption edge, with enhanced absorption extending into the visible region (400–700 nm). This shift toward longer wavelengths indicates improved visible-light harvesting ability after Ce doping (Nazarabad and Goharshadi, 2023). The redshift can be attributed to the formation of defect or impurity energy levels in the band structure of g-C_3N_4, arising from interactions between cerium species and the host matrix. Such an electronic modification is favourable for broadening the material's photoresponse range. Moreover, no distinct additional absorption peak was observed for Ce-g-C_3N_4, which may be due to the low concentration of Ce species in the composite (Barman and Sadhukhan, 2022).

The optical band gap values of the prepared samples were estimated using Tauc's relation (Eq. 3), considering a direct band gap transition (n = 2):

$$(\alpha h_v)n = A(h_v - E_g) \quad \ldots (3)$$

where α is the absorption coefficient, A is a constant, E_g is the average band gap energy of the material, n represents the type of electronic transition, and h_v is the photon energy.

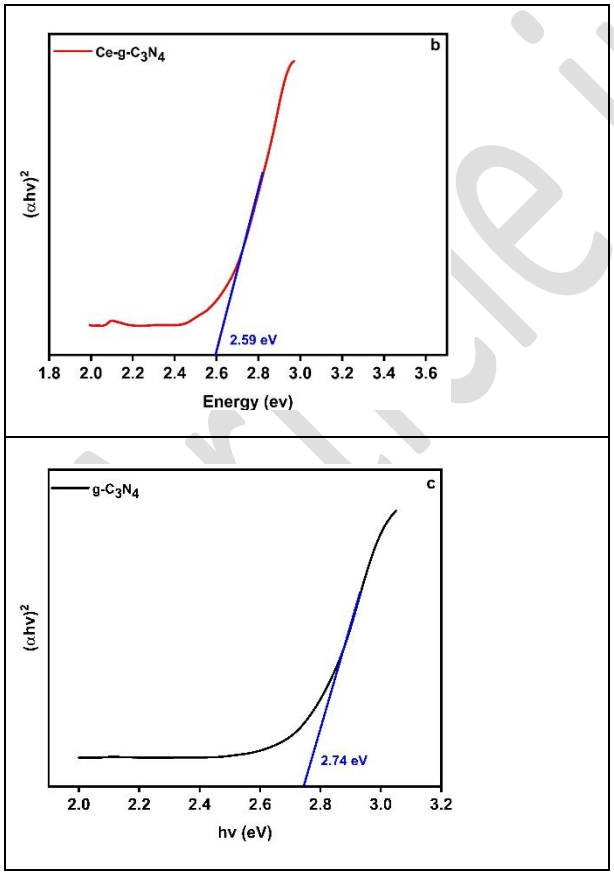

Fig. 3: b&c: shows the Tauc plots of Ce-g-C3N4 and g-C3N4 photocatalyst

The band gap values of Ce-g-C_3N_4 and g-C_3N_4 were determined to be 2.59 and 2.74 eV, respectively. The reduction in band gap after Ce incorporation indicates the formation of additional electronic states near the conduction or valence band edges. As a result, the composite can absorb lower-energy photons and utilize a larger fraction of the visible-light spectrum. The enhanced light-harvesting ability increases the generation of photogenerated electron-hole pairs under visible-light irradiation. In addition, the presence of Ce^{3+}/Ce^{4+} redox centres can facilitate electron trapping and retard charge carrier recombination. Therefore, the narrowed band gap, together with improved charge separation, is responsible for the enhanced photocatalytic degradation of RhB observed for Ce-g-C_3N_4 (Idrees *et al.* 2025; Dhilip *et al.* 2026; Karazhanov *et al.* 2009).

The enhanced photocatalytic performance of Ce-g-C_3N_4 can be attributed to the structural and optical modifications induced by Ce incorporation. XRD analysis confirmed the successful formation of the Ce-g-C_3N_4 heterojunction, while UV-visible studies revealed improved visible-light absorption via band-gap narrowing. The rough and fragmented morphology observed by SEM may expose more accessible surface sites for adsorption and photocatalytic reactions. Furthermore, the Ce^{3+}/Ce^{4+} redox couple can serve as an electron trapping centre, facilitating charge separation and suppressing electron-hole recombination. The combined effects of enhanced light harvesting, improved charge migration, and increased availability of reactive sites account for the superior photocatalytic activity of Ce-g-C3N4 relative to pristine g-C_3N_4.

3.4 Photoluminescence Studies

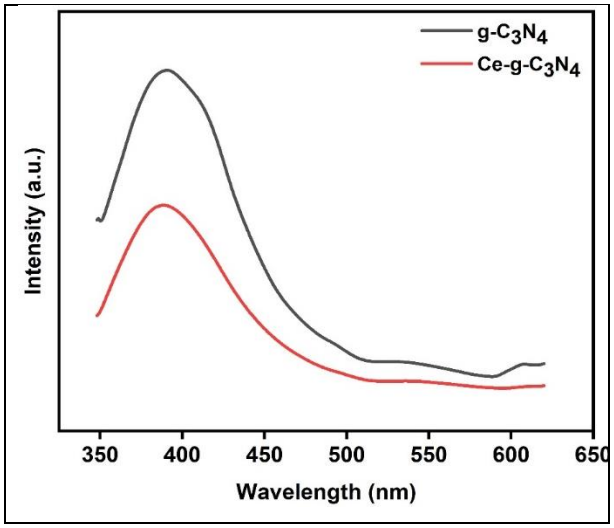

Fig. 4: shows the PL spectra of g-C3N4 and Ce-g-C3N4 composite

The PL spectra of g-C_3N_4 and Ce-g-C_3N_4 are shown in Fig. 4. Pristine g-C_3N_4 exhibits a relatively strong emission intensity, indicating rapid recombination

of photogenerated electron-hole pairs. In contrast, the emission intensity of Ce-g-C_3N_4 is considerably suppressed, suggesting that the incorporation of Ce effectively inhibits charge carrier recombination. The Ce^{3+}/Ce^{4+} redox couple can act as an electron trapping centre and prolong the lifetime of the charge carriers. The reduced recombination behaviour is consistent with the improved visible-light absorption observed from UV-visible analysis and the enhanced photocatalytic degradation of RhB. Similar observations have been reported for Ce-modified g-C_3N_4 systems, where the decrease in PL intensity was attributed to efficient charge separation and improved photocatalytic activity (Guo *et al.* 2021; Pan *et al.* 2020).

3.5 Electrochemical Impedance Spectroscopy

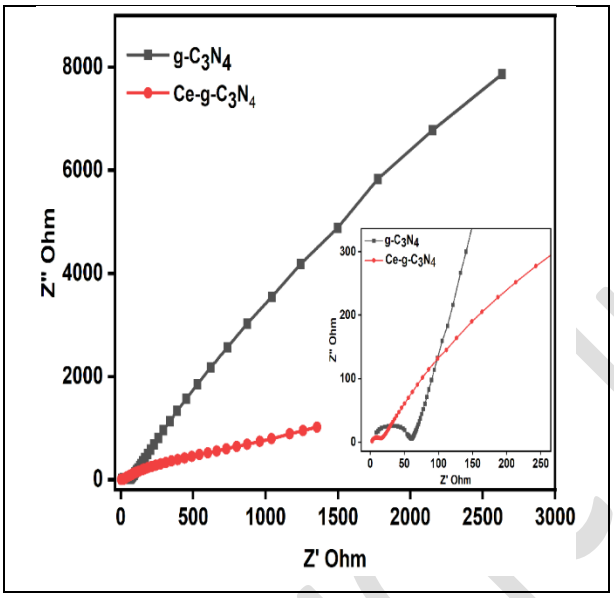

Fig. 5: shows the Nyquist plots obtained from EIS analysis of g-C_3N_4 and Ce-g-C_3N_4 composite

Electrochemical impedance spectroscopy was further employed to investigate the charge transfer characteristics of the prepared photocatalysts. As shown in Fig. 5, Ce-g-C_3N_4 exhibits a smaller semicircle diameter than pristine g-C_3N_4, indicating lower charge transfer resistance and faster interfacial electron migration. The improved charge transport behaviour confirms the strong electronic interaction between Ce species and the g-C_3N_4 matrix (Tamilselvan *et al.* 2019). The EIS results agree well with the PL analysis, which revealed suppressed electron-hole recombination after Ce incorporation. The efficient separation and migration of photogenerated charge carriers facilitate the formation of reactive oxygen species, particularly hydroxyl radicals, which were identified as the dominant active species in the scavenger experiments. Consequently, Ce-g-C_3N_4 exhibited superior photocatalytic performance, achieving 89.1% RhB degradation with an apparent rate constant of 0.0324 min^{-1} under visible-light irradiation.

3.6 SEM Analysis

The surface morphology of pristine g-C_3N_4 and Ce-g-C_3N_4 composite was examined using scanning electron microscopy (SEM), and the corresponding images are shown in Fig. 6a–c. The SEM images of pure g-C3N4 (Fig. 6a & b) reveal an irregular, bulky structure composed of densely agglomerated layered sheets. Such a stacked morphology is commonly associated with the thermal polymerization of melamine, resulting in compact layered assemblies. In contrast, the Ce-g-C_3N_4 composite (Fig. 6c) retains the layered nature of g-C_3N_4 but exhibits a rougher, more organized, and stratified surface with fragmented sheet-like features. The modified morphology suggests that the incorporation of Ce species influences the growth and stacking behaviour of g-C_3N_4 during synthesis, resulting in a rougher, more fragmented surface. This characteristic promotes efficient dye adsorption and improves photocatalytic performance.

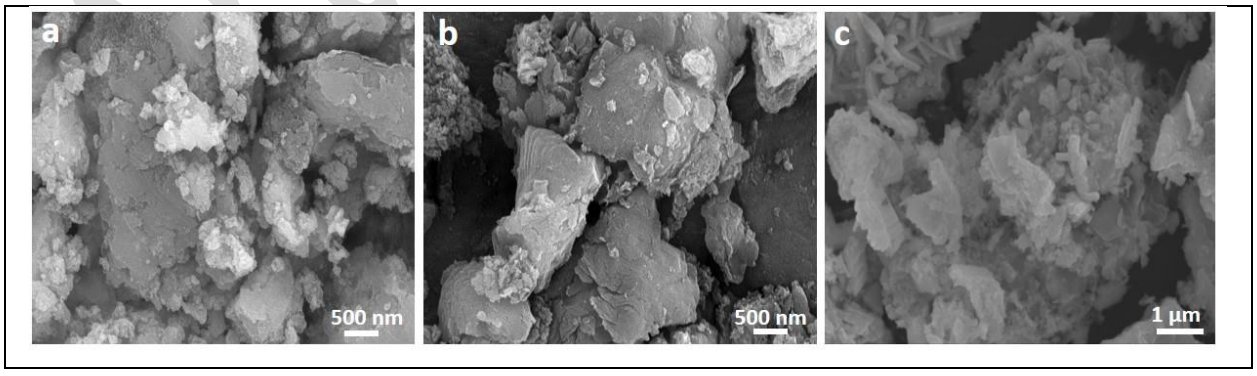

Fig. 6: (a&b) Shows the SEM images of g-C_3N_4 and (c) Ce-g-C_3N_4 composite

3.7 Energy Dispersive X-Ray Spectroscopy Analysis

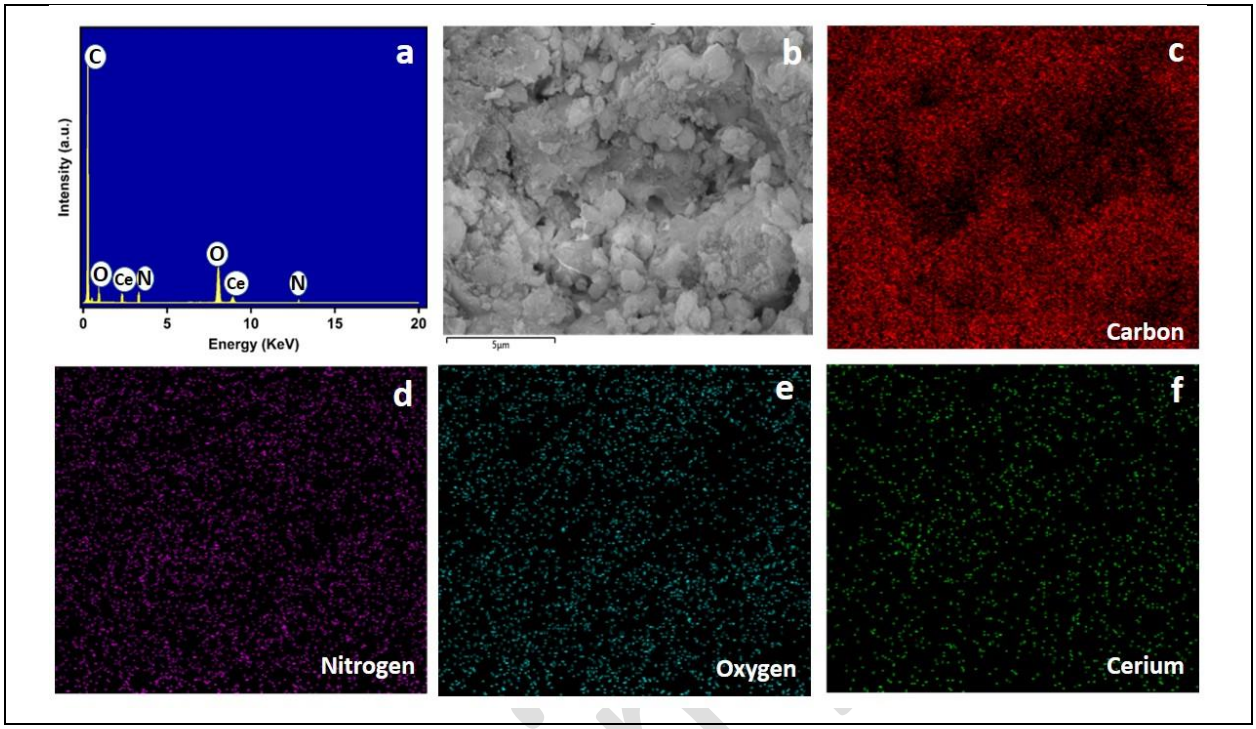

Fig. 7: (a) shows the EDS spectra of the Ce-g-C_3N_4 composite, and (b-f) show the elemental mapping of the Ce-g-C_3N_4 composite

The elemental composition of the Ce-g-C_3N_4 composite was further examined by energy-dispersive X-ray spectroscopy (EDX). As shown in Fig. 7a, well-defined signals corresponding to carbon, nitrogen, oxygen, and cerium were clearly observed. The presence of these elements confirms the successful incorporation of cerium into the g-C_3N_4 framework.

Elemental mapping analysis was also conducted to assess the spatial distribution of constituent elements within the composite. The mapping images shown in Fig. 7b–f demonstrate the presence and uniform distribution of carbon, nitrogen, oxygen, and cerium in the Ce-g-C_3N_4 composite. In particular, the homogeneous dispersion of cerium indicates effective integration of the dopant species within the composite structure.

3.8 Photocatalytic Performance Evaluation

Rhodamine B (RhB) is widely present in textile effluents and is commonly used as a model pollutant in wastewater treatment studies to evaluate photocatalytic efficiency. In addition, it has been extensively employed as a photosensitizer in dye-sensitized solar cell research. In the present work, a solution of pure RhB dye was prepared to investigate its photocatalytic degradation under visible-light irradiation.

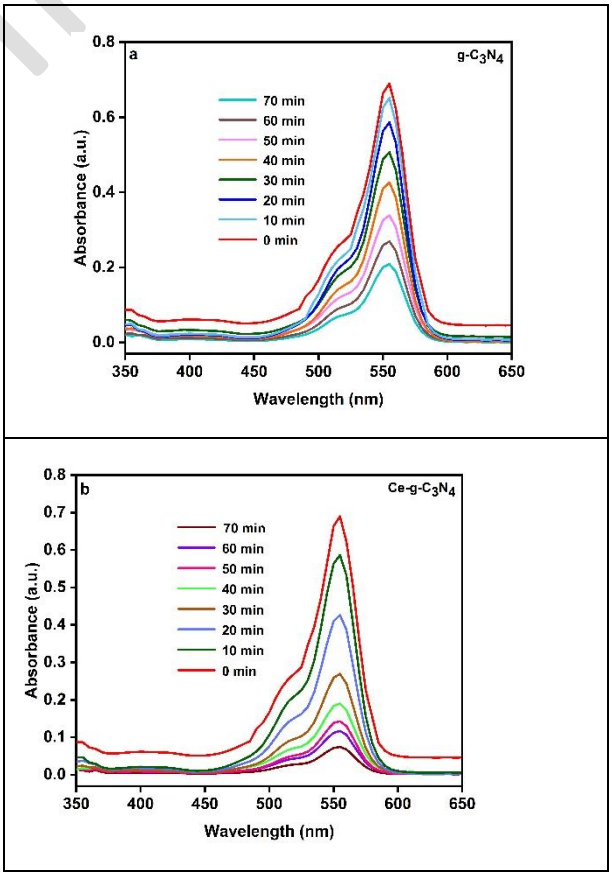

3.8.1 Impact of Irradiation Time on Photodegradation of RhB

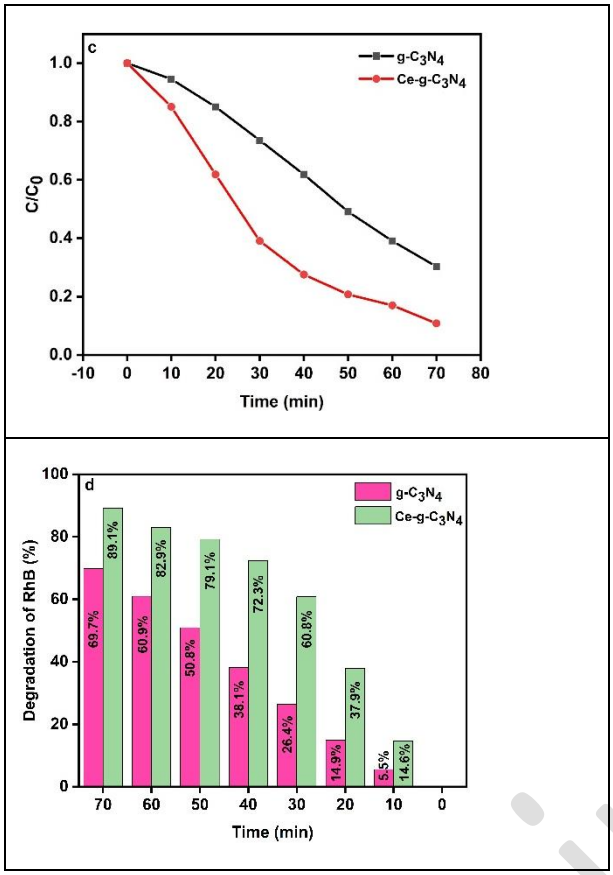

Fig. 8: a&b show UV–Vis spectra of RhB during photodegradation using g-C3N4 and Ce-g-C3N4 composite, c&d) RhB degradation efficiency as a function of irradiation time under visible-light irradiation

The variation in the absorption of the RhB dye solution before and after visible-light irradiation at different time intervals was analysed using UV–visible spectroscopy, and the results are presented in Fig. 8a,b. The characteristic absorption peak observed at 544 nm in the absence of photocatalyst corresponds to the chromophore structure of RhB. A gradual decrease in the intensity of this peak with irradiation time in the presence of photocatalysts confirms the progressive degradation of the dye molecules through photocatalytic oxidation.

The change in degradation efficiency with irradiation time is further illustrated in Fig. 8c,d. Pristine g-C_3N_4 shows comparatively lower photocatalytic activity, whereas the Ce-g-C_3N_4 composite exhibits significantly higher performance under identical experimental conditions. The degradation results indicate that g-C_3N_4 and Ce-g-C_3N_4 achieve 5.5% and 14.6% removal, respectively, within the first 10 min of irradiation. With continued exposure, the degradation efficiency increases to 69.7% for g-C_3N_4 and 89.1% for Ce-g-C_3N_4 after 70 min under visible light. The improved photocatalytic activity of Ce-g-C_3N_4 can be attributed to the synergistic effect between cerium species and the g-C_3N_4 framework, which facilitates charge separation and suppresses electron-hole recombination. In addition, the presence of Ce contributes to a higher density of active sites and improved interaction with dye molecules, leading to enhanced degradation efficiency (Khan *et al.* 2025).

3.8.2 Effect of pH

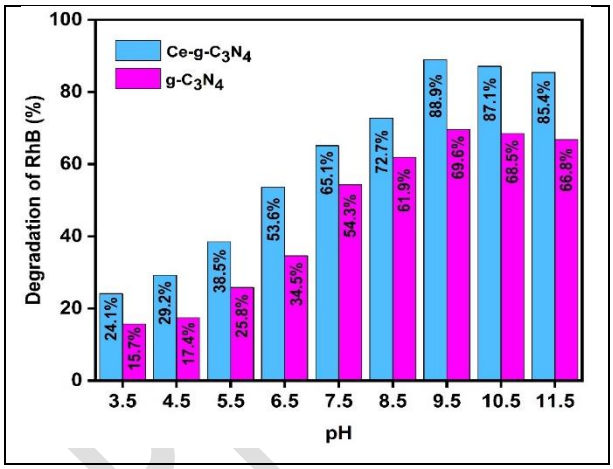

Fig. 9: RhB degradation efficiency as a function of pH under visible-light irradiation

The photocatalytic efficiency of a system is strongly influenced by the pH of the aqueous medium. In particular, pH governs both the photocatalyst's surface charge and the dominant reactive species involved in the degradation process. At lower pH values, photogenerated holes (h^+) tend to play a major role in oxidation reactions, whereas hydroxyl radicals (•OH) become more significant under neutral to alkaline conditions.

The surface charge behaviour of the catalyst can be explained based on its point of zero charge (pH_pzc). When the solution pH is lower than the pH_pzc, the catalyst surface becomes positively charged, favouring electrostatic attraction towards anionic species and repulsion of cationic species. In contrast, at pH values above pH_pzc, the surface acquires a negative charge, which enhances interactions with cationic pollutants and reduces repulsion. In the present study, the pH-dependent photocatalytic degradation of RhB was investigated while other parameters were held constant. The catalyst dosage was maintained at 30 mg, and the initial dye concentration was fixed at 50 ppm for both g-C_3N_4 and Ce-g-C_3N_4, with an irradiation time of 70 min. Since RhB is a cationic dye, it becomes positively charged upon dissociation in water. The pH_pzc of Ce-g-C_3N_4 was determined to be 6.2.

At pH values below pH_pzc, the positively charged catalyst surface repels RhB molecules, thereby reducing adsorption and limiting the formation of reactive hydroxyl radicals, resulting in lower degradation efficiency. In contrast, under alkaline conditions (pH > 6.2), the catalyst surface becomes negatively charged,

thereby enhancing electrostatic attraction to RhB molecules and improving their adsorption on the surface. This condition also promotes the generation of reactive species, thereby increasing photocatalytic activity. Accordingly, the highest degradation efficiency of 88.9 % was achieved for Ce-g-C_3N_4 at pH 9.5 after 70 min of visible-light irradiation, as shown in Fig. 9. Under the same conditions, pristine g-C_3N_4 showed a comparatively lower degradation efficiency of 69.6 % (Ahmad *et al.* 2016; Rafiq *et al.* 2021).

3.8.3 Effect of Catalyst Concentration

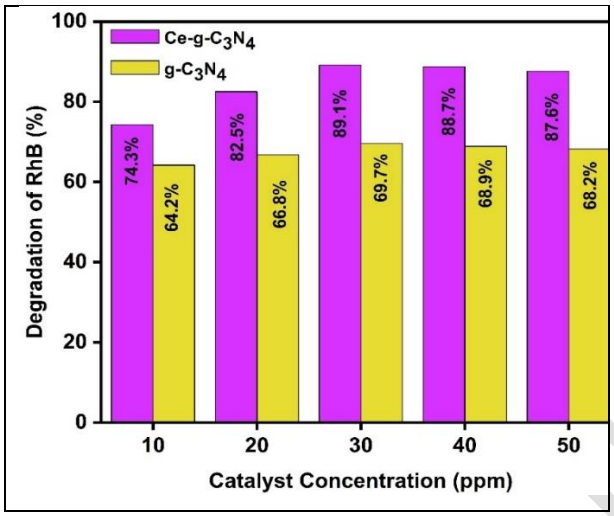

Fig. 10: Effect of catalyst concentration on RhB degradation efficiency under visible-light irradiation

The efficiency of photocatalytic degradation is strongly dependent on the catalyst dosage in the reaction medium. To examine this effect, the degradation of 50 ppm RhB solution was investigated at different catalyst loadings (10, 20, 30, 40, and 50 mg), while keeping other parameters constant (pH = 9.5, irradiation time = 70 min, and identical experimental conditions for both g-C_3N_4 and Ce-g-C_3N_4 systems). As shown in Fig. 10, the degradation efficiency increases with catalyst loading from 10 to 30 mg. This enhancement is attributed to the availability of more active surface sites, which promotes the formation of reactive oxygen species, particularly hydroxyl radicals, thereby accelerating the degradation process. Ce-g-C_3N_4 exhibits its maximum activity at 30 mg, indicating an optimum catalyst dose for efficient RhB removal.

However, further increase in catalyst concentration beyond the optimum value leads to a gradual decrease in degradation efficiency. This reduction can be explained by increased turbidity of the suspension, which limits light penetration and reduces photon absorption by the catalyst surface. In addition, higher catalyst loading promotes particle agglomeration, which reduces the effective surface area and limits the formation of reactive species, ultimately lowering photocatalytic performance (Abdellah *et al.* 2018).

3.8.4 Effect of Initial Dye Concentration

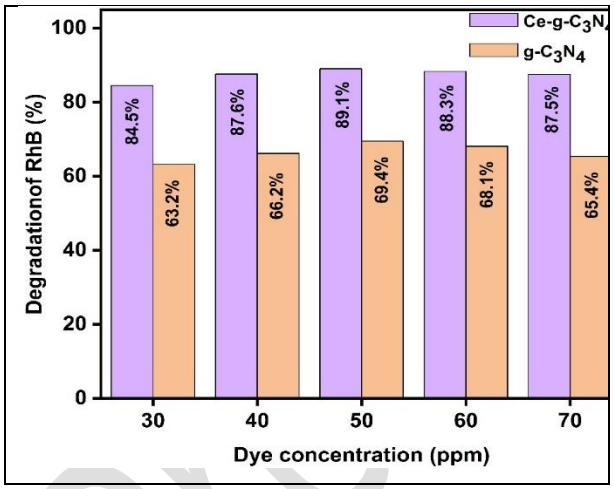

Fig. 11: Effect of dye concentration on RhB degradation efficiency under visible-light irradiation

During the photocatalytic process, the adsorption of dye molecules on the catalyst surface plays a more important role than their presence in the bulk solution. Therefore, the initial dye concentration significantly influences the overall degradation efficiency under constant catalyst loading.

As shown in Fig. 11, the photocatalytic efficiency decreases with increasing RhB concentration beyond the optimum level. All samples exhibit maximum degradation at 50 ppm under their respective optimized pH and catalyst dosage conditions. At this concentration, Ce-g-C_3N_4 achieves the highest degradation efficiency of 89.1%. The decline in performance at higher dye concentrations can be attributed to an increased number of dye molecules occupying active sites on the catalyst surface, thereby limiting the availability of sites for photon absorption. In addition, the dense dye solution reduces light penetration, thereby decreasing the number of photons reaching the catalyst surface. This results in reduced generation of reactive species, such as hydroxyl radicals, which ultimately slows the decolorization process. Similar behaviour has been reported previously, in which an increase in dye concentration led to a decrease in the photocatalytic rate due to reduced light transmission and a shorter photon path length within the solution (Nadeem *et al.* 2021).

3.8.5 Recyclability of the Photocatalyst

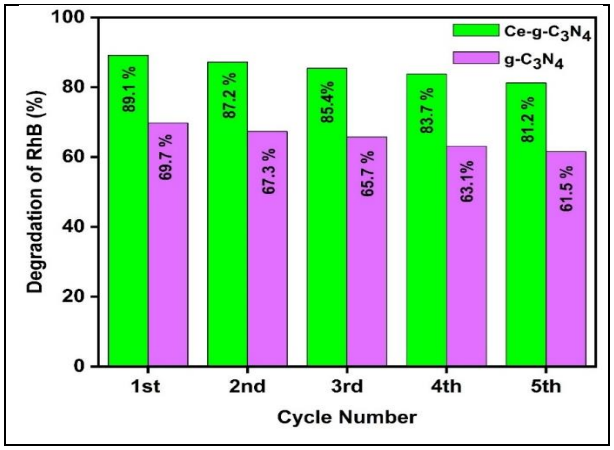

Fig. 12: Effect of repeated cycles on the photodegradation efficiency of RhB by g-C3N4 and Ce-g-C3N4

The stability of g-C_3N_4 and Ce-g-C_3N_4 was evaluated through five successive photocatalytic cycles for RhB degradation, as shown in Fig. 12. The results indicate that g-C_3N_4 and Ce-g-C_3N_4 retain degradation efficiencies of 61.5% and 81.2%, respectively, after five cycles, compared with their initial efficiencies of 69.7% and 89.1%. The slight decline in activity can be attributed to partial blockage of active sites by intermediate species and minor loss of catalyst during the recovery process. Despite this decrease, the Ce-g-C_3N_4 composite maintains a relatively high activity level, indicating good structural integrity and stability under repeated irradiation conditions.

These results confirm that the prepared nanocomposite possesses stable photocatalytic behaviour and can be effectively reused for multiple cycles without significant loss of performance, supporting its potential application in wastewater treatment (Abouri *et al.* 2025).

3.8.6 Scavengers Study

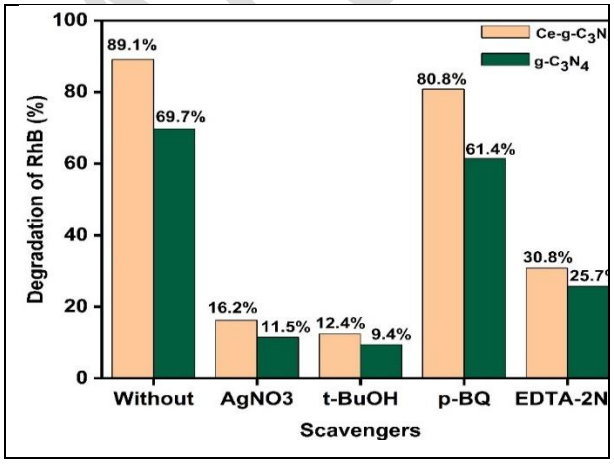

Fig. 13: Effect of different scavengers on the photocatalytic degradation of RhB

In photocatalytic oxidation, several reactive species contribute to the degradation process, including superoxide radicals (•O_2^-), photogenerated electrons (e^-), holes (h^+), and hydroxyl radicals (•OH). To identify the dominant active species involved in RhB degradation, radical-scavenger experiments were performed with specific trapping agents. p-Benzoquinone (p-BQ) was used to quench superoxide radicals, silver nitrate ($AgNO_3$) acted as an electron scavenger, disodium ethylenediaminetetraacetate (EDTA-2Na) was used to capture holes, and tert-butanol (t-BuOH) was employed as a hydroxyl radical scavenger (Li *et al.* 2025). The addition of various scavengers significantly decreased degradation efficiency, indicating that multiple reactive species participate in the photocatalytic process. In the presence of p-BQ, EDTA-2Na, $AgNO_3$, and t-BuOH, the degradation efficiency decreased to 80.8%, 30.8%, 16.2%, and 12.4%, respectively, for Ce-g-C3N4. Based on the magnitude of suppression, the contribution of the reactive species can be qualitatively ranked as •OH > e^- > h^+ > •O_2^-. The addition of tert-butanol also resulted in a significant decrease in photocatalytic activity, confirming the involvement of •OH radicals in the oxidation process. Hydroxyl radicals have a very high oxidation potential (2.8 V) and can effectively attack the chromophoric structure and intermediate products of RhB, thereby promoting their mineralization. Previous studies have reported that •OH radicals play a dominant role in the mineralization pathway of RhB and significantly contribute to its photocatalytic degradation (Ali *et al.* 2019; Mohamed and Sandhya, 2017). Although p-BQ caused a relatively small decrease in degradation efficiency, superoxide radicals are still considered important because they have a very high oxidation potential and are continuously generated via electron-mediated oxidation reactions. Therefore, although •OH radical is the major active species in the present system, the contribution of •O_2^- radicals to the degradation and mineralization of RhB cannot be neglected.

3.8.7 Kinetic Model Study

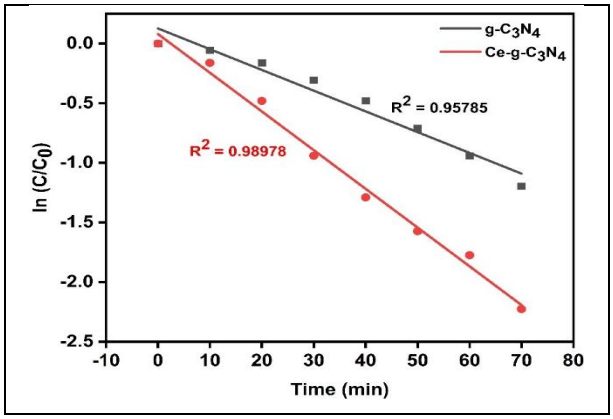

Fig. 14: Photodegradation of RhB over photocatalysts under visible light irradiation; lines represent the corresponding pseudo-first-order kinetic fits

The kinetic analysis of RhB degradation under visible-light irradiation is presented in Fig. 14, which shows the variation of $\ln(C/C_0)$ with irradiation time for both g-C_3N_4 and Ce-g-C_3N_4. The linear relationship confirms that the photocatalytic degradation follows pseudo-first-order kinetics for both systems. The Ce-g-C_3N_4 composite exhibits a higher reaction rate compared to pristine g-C_3N_4, as reflected by the calculated apparent rate constants of 0.0324 min^{-1} and 0.0173 min^{-1}, respectively. This increase indicates faster degradation kinetics and improved photocatalytic efficiency of the Ce-modified sample under identical experimental conditions.

The pseudo-first-order kinetic behaviour can be expressed using the following equation (Eq. 4):

$$-\ln(C/C_0) = k_t \quad \ldots (4)$$

where C_0 and C represent the initial and time-dependent concentrations of RhB, respectively, k is the apparent rate constant of the photocatalytic reaction, and t denotes the irradiation time. The slope of the linear fit corresponds to the apparent rate constant for both g-C_3N_4 and Ce-g-C_3N_4 systems. In particular, the Ce-g-C_3N_4 composite exhibits an apparent rate constant that is approximately three times higher than that of pristine g-C_3N_4 under visible-light irradiation, indicating a significantly faster degradation process (Gatou *et al.* 2023).

3.8.8 Stability of Ce-g-C_3N_4 Composite

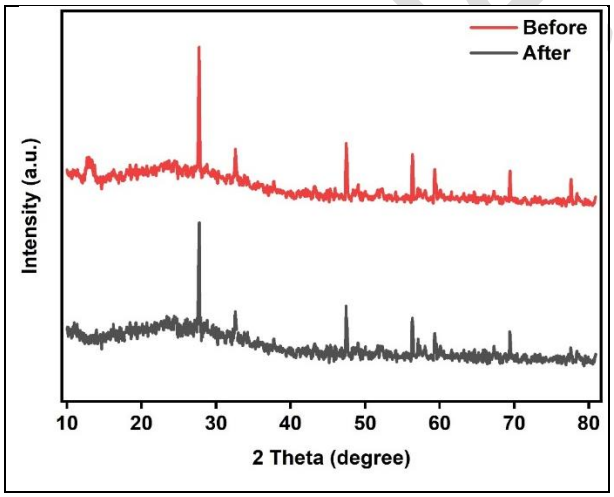

Fig. 15: XRD patterns of the Ce-g-C_3N_4 catalyst before and after the photocatalytic degradation reaction

The XRD patterns before and after the photocatalytic reaction are presented in Fig. 15. The XRD patterns recorded before and after the photocatalytic reaction exhibit diffraction peaks at nearly identical 2θ positions, indicating that the crystal structure of the catalyst is well preserved after use. Although the absence of peaks / slight reduction in the intensity of some diffraction peaks is observed after the reaction, this can be attributed to the adsorption of dye molecules or reaction intermediates on the catalyst surface, as well as minor changes in crystallinity caused by repeated irradiation and recovery. The absence of phase changes confirms that the catalyst maintains its structural integrity under the reaction conditions, which is important for achieving stable photocatalytic performance during repeated use. Similar observations have been reported for stable semiconductor photocatalysts after photocatalytic degradation, where the preservation of the crystal structure is considered an indication of good catalyst durability (Schneider *et al.* 2014; Low *et al.* 2017).

3.8.9 Photodegradation Mechanism

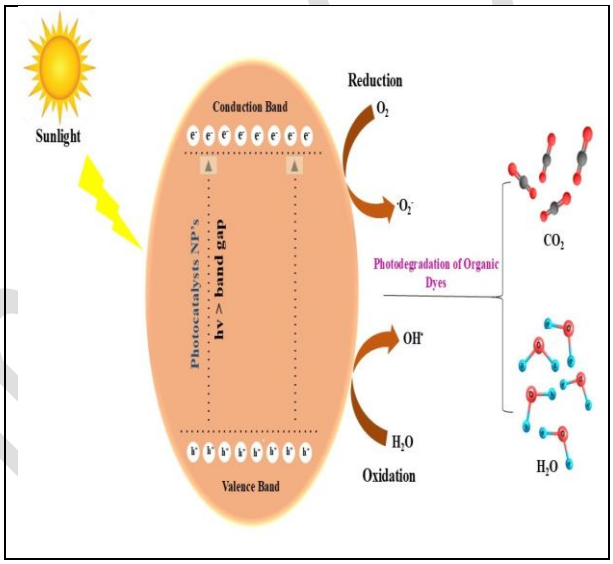

Fig. 16: Proposed mechanisms for the photocatalytic degradation of RhB

Ce doping influences the crystallite size of the samples to some extent; however, the photocatalytic activity does not follow a direct correlation with crystallite size variation. To explain the observed enhancement in photocatalytic performance under visible-light irradiation, the charge excitation and transfer mechanism between Ce and g-C_3N_4 is illustrated in Fig. 16. Upon Ce incorporation into the g-C_3N_4 framework, interfacial interactions between the dye molecules and the doped surface facilitate a photoinduced oxidation pathway. In this system, the redox couple Ce^{4+}/Ce^{3+} plays a key role by serving as an efficient electron-trapping center, thereby improving charge separation within the photocatalyst.

Under visible-light irradiation, RhB molecules may also act as photosensitizers by absorbing light energy and injecting electrons into the conduction band of g-C_3N_4. In parallel, intrinsic excitation within the photocatalyst generates electron–hole pairs when photons with energy equal to or greater than the band gap are absorbed. The photogenerated electrons migrate to

the surface and react with dissolved oxygen to form superoxide radicals ($\bullet O_2^-$), while the photogenerated holes oxidize water or hydroxyl species to produce hydroxyl radicals (•OH) (Luminita *et al.* 2022). These reactive oxygen species subsequently mineralize RhB into simpler products such as CO_2 and H_2O. The comparatively lower activity of pristine g-C_3N_4 is mainly attributed to rapid recombination of photogenerated electron–hole pairs. In contrast, the Ce-g-C_3N_4 composite exhibits enhanced performance owing to efficient electron trapping by Ce species, which suppresses recombination and prolongs charge-carrier lifetime. This mechanism is consistent with the formation of superoxide radicals via molecular oxygen, as reported earlier. The proposed photocatalytic pathway for RhB degradation is illustrated in Fig. 16.

$$\text{Ce-g-}C_3N_4 + h_v \longrightarrow \text{Ce-g-}C_3N_4\ (e^- + h^+)$$

$$O_2 + e^- \longrightarrow O.2^-$$

$$\bullet O_2^- + H+ \longrightarrow HOO.$$

$$2\ HOO. \longrightarrow H_2O_2 + O_2$$

$$H_2O + h^+ \longrightarrow HO. + H^+$$

$$RhB + (HOO. + HO. + H+\ H_2O_2) \longrightarrow \text{Intermediate Products} \longrightarrow CO_2 + H_2O$$

Table 1: Comparison of the photocatalytic performance of the present Ce-g-C_3N_4 composite with previously reported Ce/g-C_3N_4-based photocatalysts under visible-light irradiation

Photocatalyst	Pollutant	Light Source	Degradation Efficiency (%)	Rate Constant (min^{-1})	Reference
CeO_2/g-C_3N_4	Methyl Red	Visible light	84.5	0.021	Khansaa *et al.* (2025)
CeO_2/g-C_3N_4	2,4-Dichlorophenol	Visible light	86.0	0.025	Guo *et al.* (2021)
Ce-In_2O_3@g-C_3N_4	RhB	Visible light	91.0	0.036	Alsalmah *et al.* (2025)
Fe-Ce/g-C_3N_4	RhB	Visible light	87.0	0.028	Pan *et al.* (2020)
Ce-g-C_3N_4	RhB	Visible light	89.1	0.0324	work

A comparison with recently reported Ce/g-C_3N_4 based photocatalysts indicates that the Ce-g-C_3N_4 composite developed in this work exhibits competitive photocatalytic activity under visible-light irradiation. The observed degradation efficiency of 89.1% and the apparent rate constant of 0.0324 min^{-1} are comparable to or higher than many previously reported Ce/g-C_3N_4 systems. The enhanced performance can be attributed to the effective interfacial coupling between Ce and g-C_3N_4, improved visible-light absorption, and efficient separation of photogenerated charge carriers.

4. CONCLUSION

A Ce-g-C_3N_4 composite was successfully synthesized through a simple hydrothermal method and applied for the visible-light-driven degradation of Rhodamine B. Compared with pristine g-C_3N_4, Ce-g-C_3N_4 exhibited superior photocatalytic activity, achieving 89.1% degradation with an apparent rate constant of 0.0324 min^{-1} under the optimum conditions of 30 mg catalyst dosage, 50 ppm RhB concentration, and pH 9.5. The enhanced performance is mainly attributed to improved visible-light absorption and efficient separation of photogenerated charge carriers, as evidenced by a reduced band gap, suppressed PL intensity, and lower charge-transfer resistance as determined by EIS analysis. In addition, scavenger experiments revealed that •OH radicals are the dominant reactive species responsible for RhB degradation. The improved stability and enhanced activity at relatively high dye concentrations highlight the potential of Ce-g-C_3N_4 for practical wastewater treatment. Further studies on real wastewater matrices and long-term operation are needed to explore its large-scale environmental applications.

ACKNOWLEDGEMENT

The authors are thankful to Dr. A. Loganathan, Associate Professor, Department of Chemistry, Thiruvalluvar Government Arts College, Rasipuram, for their valuable input and guidance at various stages during the discussions.

FUNDING

This research received no specific grant from any funding agency in the public, commercial, or not-for-profit sectors.

CONFLICTS OF INTEREST

The authors declare no conflict of interest.

COPYRIGHT

REFERENCES

Abdellah, M. H., Nosier, S. A., El-Shazly, A. H. and Mubarak, A. A., Photocatalytic decolorization of methylene blue using TiO_2/UV system enhanced by air sparging, *Alex. Eng. J*., 57(4), 3727-3735(2018). https://doi.org/10.1016/j.aej.2018.07.018

Abouri, M., Benzaouak, A., Elouardi, M., Lahcen, E. H., Fatima, Z., Khalil, A., Belkheir, H., Rachid, S., Jodeh, S., Alaoui, E. B. M. and Adnane, E. H., Enhanced photocatalytic degradation of Rhodamine B using polyaniline-coated $XTiO_3$(X = Co, Ni) nanocomposites, *Sci. Rep*., 15(1), 3595 (2025). https://doi.org/10.1038/s41598-024-83610-1

Adewuyi, A. and Oderinde, R. A., Graphitic carbon nitride-modified cerium ferrite: an efficient photocatalyst for the degradation of ciprofloxacin, ampicillin, and erythromycin in aqueous solution, *J. Mater. Sci. Mater. Eng*., 19(1), 37(2024). https://doi.org/10.1186/s40712-024-00183-7

Ahmad, M., Mohammad, R. F. and Mohammad, R. M., Modified Scherrer Equation to Estimate More Accurately Nano-Crystallite Size Using XRD, *World J. Nano Sci. Eng*., 2(3), 154-160(2012). https://doi.org/10.4236/wjnse.2012.23020

Ahmad, R., Ahmad, Z., Khan, A. U., Mastoi, N. R., Aslam, M. and Kim, J., Photocatalytic systems as an advanced environmental remediation: recent developments, limitations and new avenues for applications, *J. Environ. Chem. Eng*., 4(4), 4143-4164 (2016). https://doi.org/10.1016/j.jece.2016.09.009

Ali, M. M., Arya, N. J. S. and Sandhya, K. Y., Role of reactive oxygen species in the visible light photocatalytic mineralization of rhodamine B dye by P25-carbon dot photocatalyst, *Dyes Pigm*., 163, 274–284 (2019). https://doi.org/10.1016/j.dyepig.2018.11.057

Alosaimi, E. H., Azeem, N., Tahir, N., Jilani, A., Zahid, M., Salman, A. S., Javed, I., Yaseen, M., Rehan, A. Z. and Imran, S., Investigation of Fe-Doped Graphitic Carbon Nitride-Silver Tungstate as a Ternary Visible Light Active Photocatalyst, *J. Chem.*, 2021, 4660423 (2021). https://doi.org/10.1155/2021/4660423

Alsalmah, H. A., Muhammad, A. and Sonia, Z., Multifunctional Ce-In_2O_3@ g-C_3N_4 nanocomposites: Synthesis, charge carrier engineering, and visible-light-driven photocatalysis, *Ceram. Int*., 51(26), 51327-51341(2025). https://doi.org/10.1016/j.ceramint.2025.08.359

Anjana, R, Hanamantrao, D. P., Nasrin, B. G., Raja, V., Rimal, I. R. S, Susan, J. J., Vediappan, K., Jose, P. S., Neppolian, B. and Sajan, D., Hydrothermal synthesis of graphitic carbon nitride/Ce doped Fe_2O_3 heterostructures for supercapattery device and hydrogen evolution reaction, *J. Energy Storage*., 116, 116021(2025). https://doi.org/10.1016/j.est.2025.116021

Barman, S. and Sadhukhan, M., Facile bulk production of highly blue fluorescent graphitic carbon nitride quantum dots and their application as highly selective and sensitive sensors for the detection of mercuric and iodide ions in aqueous media, *J. Mater. Chem*., 22(41), 21832-21837 (2022). https://doi.org/10.1039/C2JM35501A

Dhilip, P., Mahalingam, P., Mohandas Gandhi, A. S., Rajesh, A., Sandhiya, A. and Rajasekaran, D., Synthesis and Characterize the Supercapacitor Performance of WO_3/rGO, WO_3/rGO/WO_3, and $NiWO_4$/rGO/$NiWO_4$ Composites, *Chem. Select*, 11(9), e04684(2026). https://doi.org/10.1002/slct.202504684

Kalaiyarasi, C., Dhilip, P., Dhivya, A., and Sivakumar, P., Photocatalytic degradation of Rhodamine B dye: MWCNT, ZrO_2/MWCNT and Y-ZrO_2/MWCNT hybrid composites as potential photocatalysts, Ionics. (2026). https://doi.org/10.1007/s11581-026-07270-z.

Devi, N. S., Devi, R. R., Kumar, A. N., Rekha, P., Kovendhan, M., Lorena, C. P. and Thanikaikarasan, S., Facile co-precipitation synthesize of CeO_2@g-C_3N_4 heterostructure for sustainable sunlight photodegradation of organic dyes and antibacterial activity, *Chem. Pap*., 80(4), 3941-3959(2026). https://doi.org/10.1007/s11696-026-04663-2

Gatou, M. A., Fiorentis, E., Lagopati, N. and Evangelia A. P., Photodegradation of Rhodamine B and Phenol Using TiO_2/SiO_2 Composite Nanoparticles: A Comparative Study, *Water*, 15 (15), 2773(2023). https://doi.org/10.3390/w15152773

Guo, L., Yang, J., Zhang, H., Wang, R., Xu, J. and Wang, J., Highly Enhanced Visible-Light Photocatalytic Activity via a Novel Surface Structure of CeO_2/g-C_3N_4 toward Removal of 2,4-Dichlorophenol and

Cr(VI), *ChemCatChem*, 13(8), 2034–2044 (2021). https://doi.org/10.1002/cctc.202001939

Idrees, I., Zafar, M., Umer, M., Rehman, F., Razzaq, A., Kim, S., Yang, Y. and Kim, W. Y., Silver (Ag) doped graphitic carbon nitride (g-C_3N_4) photocatalyst for enhanced degradation of Ciprofloxacin (CIP), *Res. Phys*., 68, 108071(2025). https://doi.org/10.1016/j.rinp.2024.108071

Kesarla, M. K., Torres, M. O. F., Ramos, M. A. A., Chi, F. O., González, C. G. E., Aleman, M., Torres, J. T., and Godavarthi, S., Synthesis of g-C_3N_4/N-doped CeO_2 composite for photocatalytic degradation of an herbicide, *J. Mater. Res. Technol*., 8(2), 1628-1635(2019). https://doi.org/10.1016/j.jmrt.2018.11.008

Khan, S., Kim, D. S., Ullah, M., Sadiq, M., Niaz., M., Khan, M., Noor, A. and Sadaf, Q., Photocatalytic degradation of Rhodamine B dye over Ni–Cd doped and co-doped ZnO nanoparticles, *Sci. Rep*., 15(1), 31947 (2025). https://doi.org/10.1038/s41598-025-17684-w

Khansaa, A. E., Ethar, M. A. E., Alaa, Q., Suhad, A. I., Solhe, F. A. and Ola, A. F., Graphitic Carbon Nitride/CeO_2 Nanocomposite for Photocatalytic Degradation of Methyl Red, *Water*, 17(2), 158(2025). https://doi.org/10.3390/w17020158

Li, L., Jianhua, W. and Fang, H., Fabrication of $ZnFe_2O_4$@g-C_3N_4 for enhanced photo-fenton effect and visible light-driven organic dye degradation, *Sci. Rep*., 15(1), 21707 (2025). https://doi.org/10.1038/s41598-025-05096-9

Low, J., Yu, J., Jaroniec, M., Wageh, S. and Al-Ghamdi, A. A., Heterojunction photocatalysts, *Adv. Mater*., 29(20), 1601694 (2017). https://doi.org/10.1002/adma.201601694

Luminita, A., Lelis, M., Enesca, A. and Smagul, K., Photocatalytic activity of defective black titanium oxide photocatalysts towards pesticide degradation under UV/VIS irradiation, *Surf. Interf*., 32, 102123(2022). https://doi.org/10.1016/j.surfin.2022.102123

Manoj, K., Vijay, P. S., Shahnaz, B. B. and Raj, K., Environmental risks of textile dyes and photocatalytic materials for sustainable treatment: current status and future directions, *Discov. environ*., 3, 132(2025). https://doi.org/10.1038/s41598-024-53626-8

Mohamed, M. A. M. and Sandhya, K. Y., A Novel Approach for P25-Carbon Dot Composite and the Reactive Oxygen Species Involved in the Visible Light Photocatalytic Mineralization of Rhodamine B, *Chem. Select*, 2(35), 11840–11845 (2017). https://doi.org/10.1002/slct.201702498

Nadeem, N., Zahid, M., Rehan, Z. A. and Hanif, M. A., Improved photocatalytic degradation of dye using coal fly ash-based zinc ferrite (CFA/$ZnFe_2O_4$) composite, *Int. J. Environ. Sci. Technol*., 19(4), 3045-3060(2021). https://doi.org/10.1007/s13762-021-03255-9

Nazarabad, M. K. and Goharshadi, E. K., Ag and Ni doped graphitic carbon nitride coated on wood as a highly porous and efficient photoabsorber in interfacial solar steam generation, *J. Porous, Mater*., 30(6), 1835-1842(2023). https://doi.org/10.1007/s10934-023-01468-6

Pan, T., Dongdong, C., Jianzhang, F., Kun, W., Weihua, F., Ximiao, Z. and Zhanqiang, F., Facile synthesis of iron and cerium co-doped g-C_3N_4 with synergistic effect to enhance visible-light photocatalytic performance, *Mater. Res. Bull*, 125, 110812(2020). https://doi.org/10.1016/j.materresbull.2020.110812

Pattanayak, S. D., Surana, M., Kumar, A., Dhananjay, S. and Dharm, P., Graphitic carbon nitride(g-C_3N_4)-based photocatalysts for dye removal: Current status, *Sustain. Chem. Environ*., 7, 100141(2024). https://doi.org/10.1016/j.scenv.2024.100141

Pratikshya, D., Sulagna, P., Sonali, P., Bhagyashree, P. and Kulamani, P., Alkali metal-doped g-C_3N_4: a multifunctional photocatalytic platform for solar-induced energy conversion and environmental restoration, *EES Catal.*, 4(2), 286-332(2026). https://doi.org/10.1039/D5EY00306G

Rafiq, A., Ikram, M., Ali, S., Niaz, F., Khan, M., Khan, Q. and Maqbool, M., Photocatalytic degradation of dyes using semiconductor photocatalysts to clean industrial water pollution, *J. Ind. Eng. Chem*., 97, 111-128, (2021). https://doi.org/10.1016/j.jiec.2021.02.017

Karazhanov, S. Z., Ravindran, P., Fjellvag, H. and Svensson, B. G., Electronic structure and optical properties of $ZnSiO_3$ and Zn_2SiO_4, *J. Appl. Phys.*, 106(12), 123701 (2009). https://doi.org/10.1063/1.3268445

Schneider, J., Matsuoka, M., Takeuchi, M., Zhang, J., Horiuchi, Y., Anpo, M. and Bahnemann, D. W., Understanding TiO_2 photocatalysis: Mechanisms and materials, *Chem. Rev*., 114(19), 9919–9986 (2014). https://doi.org/10.1021/cr5001892

Tamilselvan, A., Chandrasekar, M. S., Rajesh, K., Smagul, K. and Balakumar, S., Electrochemmical performance of nitrogen doped tio2 nanotubes as electrode materials for supercapacitor and Li-ion battery, *Mol.*, 24(16), 2952(2019). https://doi.org/10.3390/molecules24162952

Wudil, Y. S., Ahmad, U. F., Gondal, M. A., Mohammed, A. A, Almohammedi, A., Said, R. S., Hrahsheh, F., Haruna, K. and Mohamed, M. J. S., Tuning of graphitic carbon nitride (g-C_3N_4) for photocatalysis: a critical review, *Arab. J. Chem*., 16(3), 104542(2023). https://doi:10.1016/j.arabjc.2023.104542